

ASSESSMENT OF CELLULOSE NANOFIBERS FROM BOLAINA BLANCA WOOD OBTAINED AT THREE SHAFT HEIGHTS

Sergio Andre Arango-Perez^{1,}*

<https://orcid.org/0000-0001-8837-7301>

Héctor Enrique Gonzales-Mora¹

<https://orcid.org/0000-0002-8455-3432>

Silvia Patricia Ponce-Alvarez²

<https://orcid.org/0000-0003-1583-7113>

Abel Aurelio Gutarra-Espinoza²

<https://orcid.org/0000-0002-4955-419X>

Aldo Joao Cárdenas-Oscanoa¹

<https://orcid.org/0000-0003-3093-8414>

ABSTRACT

Cellulose nanofibers (CNF) could be obtained from diverse lignocellulosic sources, among them wood. Regarding this, it is important to clarify if the shaft section of the tree could influence the CNF characteristics. This study evaluated cellulose nanofibers from *Guazuma crinita* (bolaina blanca) obtained at different heights of the longitudinal axis of the shaft of trees from a three-and-a-half-year-old plantation.

The wood was subjected to pulping, bleaching and subsequent mechanical milling using a Changsha Samy XYQM-2L planetary ball mill to obtain cellulose nanofibers. The product was characterised using analytical techniques: scanning electron microscopy, X-ray diffraction, thermogravimetric analysis, Fourier transform infrared spectroscopy, ultraviolet–visible spectroscopy. Additionally, the degree of polymerisation was determined. The effect of longitudinal position on cellulose nanofibers characteristics was evaluated by comparing means using ANOVA and Kruskal–Wallis statistical tests. The yield of cellulose nanofibers production from the high, middle and basal sections was 32,1 %, 33,6 % and 31 %, respectively. The obtained cellulose nanofibers exhibited a significantly larger diameter for the high zone (84 nm) compared with the middle (75 nm) and basal (69 nm) zones; the length remained above the micrometre range. With respect to degree of polymerisation, a decrease was evidenced with respect to the increase in shaft height; the basal zone exhibited a degree of polymerisation of 300, a significantly higher value than the middle and high zones, which exhibited degree of polymerisation of 249 and 211, respectively. The product showed typical cellulose type I polymorphism and crystallinity indexes of 76 %, 93 % and 96 % for the high, middle and basal sections, respectively. Regarding the thermostability of cellulose nanofibers, the maximum degradation rate of cellulose nanofibers occurred between 335 °C and 341 °C, with cellulose nanofibers from the basal area being the most stable. The adsorption of the methylene blue dye on cellulose nanofibers was evaluated; an efficiency > 60 % was found.

Keywords: Bolaina blanca, cellulose nanofibers, *Guazuma crinita*, polimerization degree, pulp treatment.

¹Universidad Nacional Agraria La Molina. Facultad de Ciencias Forestales. Departamento de Industrias Forestales. Laboratorio de Productos Forestales de Transformación Química. Lima, Perú.

²Universidad de Lima. Grupo de Nanomateriales Aplicados. Lima, Perú.

*Corresponding author: sarango@lamolina.edu.pe

Received: 08.10.2022 Accepted: 27.09.2023

INTRODUCTION

Cellulose is the most abundant renewable polymer on the planet, with an annual biosynthesis estimated at > 1011 tonnes (Habibi 2014). Owing to its natural origin and widespread availability, cellulose is used in fibre form or derived form for creating a wide range of materials and products, such as paper, composite boards, cosmetics, and food additives.

Cellulose fibre is represented at different levels. From a biological viewpoint, cellulose chains are formed by β -D-glucose units. The second level or macromolecular level comprises the union of these linear cellulose chains with each other forming the elementary fibrils or microfibrils, also known, from a technical-technological point of view, as nanocellulose. The extraction of these nanoconstituents is possible using mechanical and chemical methods or using a combination of these methods (Borjesson and Westman 2015, Kargazadeh *et al.* 2017, Siddiqui *et al.* 2011, Yildirim and Shaler 2017).

Nanocellulose (NC) has become extremely popular in different industries not only for being a biodegradable material with high availability but also for possessing interesting properties, such as high mechanical strength and low density, dielectric properties, possibility of chemical modification, dimensional stability and thermal stability (Herrera 2018, Ozen *et al.* 2021, Tárres 2017). Due to these benefits, nanocellulose is a basic material used in different industries such as: Construction/polymers, Paper industry, Cosmetics, Biomedicine and Food industry (Herrera 2018, Lee *et al.* 2012, Tárres 2017).

However, there is still insufficient knowledge concerning the potential influence of raw material sources on the final characteristics of NC. Wood is one of the main sources currently used for NC production owing to its lignocellulose composition and high availability. The most commonly used forest species are *Eucalyptus* and Pine, but there are also other alternatives such as tropical species that have adapted to a fast-growing plantation system, which is ideal for the continuous production of NC.

In this context, assessing other non-conventional potential forest sources for the creation of NC is an interesting research topic, while also posing the question of how the different heights of the longitudinal axis of the shaft influence the characteristics of NC.

Among the species used for plantation purposes, bolaina blanca (*Guazuma crinita* Lam.) stands out (Miguel *et al.* 2019, Rodríguez *et al.* 2015). This forest species is widely cultivated in the country owing to its advantage of being a fast-growing species harvestable at an early age as well as the large demand for its wood for construction, furniture and mouldings (Revilla 2015).

Considering the production potential of bolaina blanca wood as a premise, promoting its use for the creation of products other than timber is necessary. All this to create products with added value in a world market that indicates a trend in biodegradable products to reduce global pollution, besides reusing or disposing waste in other ways owing to its organic origin (Trache *et al.* 2020).

MATERIALS AND METHODS

Collection and preparation of raw material

The material was extracted from three randomly selected trees with no signs of disease from a three-and-a-half-year-old plantation located in the province of Padre Abad, Department of Ucayali, Peru. A total of 58 kg of debarked bolaina blanca (*Guazuma crinita* Lam.) corresponding to logs from the basal, middle and high zones was collected. Heights were assigned based on the division of the commercial length of the shaft of the tree.

Wood samples were subjected to natural drying up to a humidity of 20 %. The material was chipped to obtain chips with 15 mm length and 5 mm width. A total of 7 kg of wood extracted from the most central part of each of the basal, middle and high sections was used.

Chemical characterisation of *Guazuma crinita* wood

The wood was sawed according to the origin of the longitudinal section to obtain sawdust, which was sieved and prepared for chemical characterisation tests. The content of the extractives was determined according to the TAPPI T 204 cm-97 standard (2007), using 96 % ethyl alcohol for extraction. The holocellu-

lose and cellulose contents were obtained using the Jayme-Wise and Kurnchner-and-Hoffer methods, respectively. Hemicellulose content was found by subtracting holocellulose and cellulose contents.

Lignin content was determined using the Klason method according to the TAPPI T 222 om-98 standard (1998). Moreover, the TAPPI T 211 om-93 standard (1993) was used for ash.

Obtaining and bleaching cellulosic pulp

The cellulosic pulp was obtained via alkaline digestion. This process was performed in triplicate for each section of interest, using a total of 5,4 kg of dry wood mass.

A total of 600 g of dry mass of wood chips for each section of study were moistened via immersion for 24 hours at room temperature, prior to the cooking process. Cooking was conducted using 18 % NaOH and 0,1 % anthraquinone (percentages corresponding to the dry mass of wood), a liquor/wood weight ratio of 4:1 and an H-factor of 1200. The pulping was conducted in a 15 L rotary digester at a defined pressure from 6 kg/cm² to 10 kg/cm² and a maximum temperature of 180 °C for 3 hours. The chemical pulping yield was determined after washing the pulp.

The bleaching process was conducted on approximately 2,4 kg total dry mass of cellulosic pulp obtained previously.

The pulps were bleached in polyethylene bags placed in a water bath and underwent a sequence of four bleaching stages. Table 1 shows the parameters used during the bleaching stages.

Table 1: Bleaching sequence.

SEQUENCE / REAGENT	D (ClO ₂)	E (NaOH)	H (NaClO)	P (H ₂ O ₂)
No. of repetitions	2	1	1	1
Bleach distribution (%)	6	5	20	2
Temperature (°C)	70	70	45	70
Time (minutes)	60	120	150	90
Consistency (C%)	8	8	8	10
pH	< 4	> 11	9 – 11	10 – 11

Bleach distribution corresponds to percentage of the dry mass of the pulp. At the end of each sequence, the pulp was washed with deionised water to neutralise the reagents used. Approximately 32 L of deionised water was used.

The amount of residual lignin in the pulps obtained before and after bleaching was evaluated using the micro-Kappa index according to the TAPPI T 236 cm-85 standard (1993b).

Measurement of anatomical elements of interest in fibres of *Guazuma crinita*

The anatomical characterisation of bolaina blanca fibres was performed from the cellulosic pulp. The length, width and wall thickness of 30 fibrous bundles were evaluated. This evaluation was performed according to the standard procedures for wood anatomy studies (IBAMA 1991) using a LEICA DM500 microscope at 4X, 10X and 40X magnifications.

Obtaining and lyophilising cellulose nanofibers (CNF)

CNF was obtained from the bleached pulp exposed to a 1 % consistency in water, via mechanical defibrillation using a Changsha Samy planetary ball mill model XYQM-2L, grinding speed of 300 revolutions per minute (rpm), total time of 3 hours and centripetal force of approximately 360 N.

After grinding, the obtained CNF was subjected to freeze-drying for yield calculation and characterisation. It started with the conditioning of the material using a freezing bath at - 40 °C (230-V FRYKA cooling bath model KB 18-40). Freeze-drying was conducted at a reduced absolute pressure (3 Pa) for 20 hours in a Christ Alpha 1-2 LDplus 230-V freeze-dryer.

Characterisation of CNF

Determination of degree of polymerisation (DP) of CNF

DP was determined using a capillary viscometer (Ubbelohde) to calculate the intrinsic viscosity (η) according to TAPPI T 230 om-08 (2008).

Scanning electron microscopy

The morphological analysis of CNF was performed via scanning electron microscopy (SEM) using ZEISS EVO MA10 equipment. The samples were dried at 50 °C for 24 hours to determine the diameter of the fibres through the obtained images.

Fourier transform infrared spectroscopy

A Bruker Alpha II Fourier transform infrared spectrometer (FTIR) was used to analyse the molecular vibrations of the freeze-dried CNF samples for each longitudinal section of the tree.

The attenuated total reflection method was conducted with successive scans at a resolution of 4 cm⁻¹ and wavenumbers in the 400 cm⁻¹ - 4000 cm⁻¹ range. Data were processed using FTIR software.

X-ray diffraction

A Bruker D8 ADVANCE X-ray diffractometer was used. X-rays with a wavelength of 1,5406 Å were incident on the freeze-dried CNF, for each longitudinal section of the tree. In the analysis parameters, the Bragg angle was swept in the range $6^\circ \leq 2\theta \leq 90^\circ$ with an interval of 0,01°.

The percentage crystallinity was calculated using Equation 1 according to Segal's method (Segal *et al.* 1959).

$$IC = \left(1 - \frac{I_{18}}{I_{22,6}} \right) \times 100 \quad (1)$$

Where IC is the crystallinity index; I_{18} and $I_{22,6}$ are intensities corresponding to the diffraction angles $2\theta = 18^\circ$ and $2\theta = 22,6^\circ$, which in turn correspond to the reflection planes (110) and (200), respectively.

Moreover, the average size of the cellulose crystals was determined using the Scherrer Equation 2, calculated for the intensity corresponding to the crystallographic plane (200) ($2\theta = 22,6^\circ$).

$$D = \frac{0,94\lambda}{b\cos\theta'} \quad (2)$$

Where 0,94 is the value of Scherrer's constant corresponding to the symmetry and shape of cellulose crystals, λ is the wavelength of the X-rays with a value of 1,5406 Å and b is the half-peak width (in radians).

Thermogravimetric analysis

Thermogravimetric analysis was performed individually for CNF from high and basal section using the TGA 70-LECO equipment according to ASTM D7582 (2015). Freeze-dried CNF samples weighing 1 g were placed in aluminium crucibles and subjected to analysis in the 25 °C - 900 °C range at a heating rate of 10 °C·min⁻¹.

Ultraviolet-visible (UV-Vis) spectroscopy

Measurements were performed using a Perkin Elmer Lambda 21 UV-Vis spectrophotometer to determine the adsorption capacity of lyophilised CNF for methylene blue dye. CNF was analysed at two concentrations

of methylene blue, 10 ppm and 20 ppm. Methylene blue was used as a control dye because it is water soluble and easy to detect in spectrophotometric equipment (Lermen *et al.* 2021).

In each case, a 15-mL sample of the solution was collected and placed in a tube of the same volume in duplicate. The sample was then centrifuged for 30 min at 5000 revolutions per minute (rpm) to sediment CNF particles. The liquid fraction, without the sediment, was read using the spectrophotometer; moreover, blank readings were recorded.

Experimental design

The data analysis was conducted using the longitudinal height of the trunk as the only variable, exposed at three levels: basal, middle and high sections. Eventually, the mean values were compared.

The results were evaluated using analysis of variance and the Kruskal–Wallis test and, in case of significance, the Tukey and Mann–Whitney tests were performed at a confidence level of 95 %.

RESULTS AND DISCUSSION

Chemical characterisation of *Guazuma crinita* wood

The results obtained showed no significance for macromolecular components such as cellulose, hemicellulose and lignin as well as for low molecular weight components such as extractives, ash and silica, along the longitudinal axis of the trunk for three-and-a-half-year-old bolaina blanca trees (Table 2). This indicates that the zone of the tree did not influence the contents of the chemical components of the extracted samples. The reported values agree with those reported by Córdova *et al.* (2020) for similar species and age, and Cipra Rodríguez *et al.* (2022) for same wood from 5 to 8 years.

Table 2: Chemical composition (%) of sections of *Guazuma crinita* wood.

Component (%)	High	Middle	Basal	Statistical test
Cellulose	53,30 (0,72)	52,67 (0,92)	52,54 (0,72)	ANOVA (n.s.)
Hemicellulose	24,18 (3,87)	23,76 (3,92)	24,64 (4,05)	ANOVA (n.s.)
Lignin	23,11 (1,59)	22,93 (2,23)	22,95 (1,92)	ANOVA (n.s.)
Extractives	1,71 (16,18)	1,90 (16,82)	1,75 (12,38)	ANOVA (n.s.)
Ash	0,77 (4,76)	0,8 (0,36)	0,76 (2,05)	Kruskal- Wallis (n.s.)
Silica	0,26 (17,39)	0,20 (3,66)	0,25 (20,75)	ANOVA (n.s.)

Data are expressed in percentage. Coefficient of variation (). n.s. denotes not significant.

Although no significance was found among the obtained values, the high zone exhibited slightly higher values for cellulose and lignin content. The high zone of the trunk contains a higher proportion of juvenile wood, which is characterised by the presence of more cellulose and, also, a greater chemical accessibility to extract a larger amount of lignin. The opposite occurs in the lower zone of the trunk, where the wood has a higher degree of lignification and is more reticulated (Malpartida 2010). The growth site of the species should also be considered, as it will influence the lignin constituents through its structure and chemistry (Césaire *et al.* 2019, Katahira *et al.* 2018).

The results show a low lignin concentration, which is related to the early age of the tree because, according to Zaki *et al.* (2012), this concentration increases as the tree ages owing to its need to harden and become more resistant.

A low level of extractives, < 2 %, is ideal for the pulping process. Honorato *et al.* (2015) mention that a high percentage of extractives in wood makes it an undesirable material for pulping because it negatively influences delignification during digestion and also forms coloured complexes that affect the whiteness of the pulp.

Obtaining and bleaching cellulosic pulp

The cellulosic pulp yields for the different shaft sections were in the 45 % - 47 % range, which correspond to the yield (40 % - 55 %) reported by Bajpai (2018) for soda digestion (Table 3).

Table 3: Results of the digestion and bleaching process of *Guazuma crinita* cellulosic pulp.

Shaft section	Pulping yield (%)	Bleaching yield (%)
Basal section	45,54 (n.s.) (15,45)	83,79(n.s.) (10,33)
Middle section	47,01(n.s.) (6,61)	87,53(n.s.) (6,91)
High section	45,95 (n.s.) (11,35)	85,63 (n.s.) (8,29)

Coefficient of variation (). n.s.: Not significant.

No significant differences were observed between pulping and bleaching yield averages among shaft sections.

The yield of the digestion process indicates nearly complete solubilisation of the non-cellulosic elements. According to the results listed in Table 2, bolaina blanca wood at different sections contained approximately 52 % cellulose. The low yield obtained from the pulping process in general results from the partial degradation of amorphous/soluble cellulose (beta and gamma cellulose) due to the parameters used, yielding a pulp with a high percentage of alpha-type cellulose, which is characterised by its insolubility in sodium hydroxide, stability and high crystallinity (Manzano 2021, Singh *et al.* 2021).

Bleaching yields vary between 90 % and 97 % (Bajpai 2018). The yield obtained in this study was between 82,3 % and 87,9 %. This low yield was caused by the loss of white pulp due to the intensity of bleaching with consequent removal of pulp mass, mainly residual lignin and low molecular weight carbohydrates such as hemicelluloses.

The Kappa index test indicates the delignification caused by the bleaching process. The unbleached pulp had a residual lignin content of 4,28 %, which decreased to < 1 % after bleaching. The delignification of the white pulp reached a value of 98,22 %, demonstrating the efficiency of the stepwise process.

Measurement of anatomical elements of interest *Guazuma crinita* fibres

Fibre length showed significant differences in the basal section with a value of 1322 μm with respect to the middle and high sections (Table 4). The length reached an average value of 1156 μm with respect to the three sections, which can be catalogued as medium length fibres according to the International Association of Wood Anatomy (IAWA 1989). However, the fibre diameter exhibited significant differences in the upper section, with a value of 28,77 μm , compared with the middle and basal sections; classified in the category of medium diameter fibres according to IBAMA (1991). Similar values for the species studied were reported by Córdova *et al.* (2020). Cell wall thickness averaged 3,91 μm , showing no significant differences among the three sections. Beeckman (2016) mentions that the environment influences both the growth and quality of the anatomical elements of wood, whereas Rodríguez *et al.* (2015) point out that the treatment conducted to separate the anatomical elements will have an influence on fibre measurement results.

Table 4: Measurements of bleached chemical pulp fibres.

Measurement of the fibres anatomical elements					
	High S.	Middle S.	Basal S.	Average	Test
Length (μm)	1087(b) (12,56)	1059(b) (15,87)	1322(a) (13,99)	1156	Tukey
Overall diameter (μm)	30,10(a) (16,86)	29,77(a) (20,51)	26,44(b) (22,33)	28,77	Kruskal-Wallis
Wall thickness (μm)	3,61(n.s.) (25,62)	4,39(n.s.) (30,30)	3,72(n.s.) (36,25)	3,91	ANVA
Lumen diameter (μm)	17,22(b) (10,43)	16,59(c) (20,86)	18,17(a) (35,95)	17,33	Kruskal-Wallis

Means that do not share a letter are significantly different. n.s.: Not significant. Coefficient of variation (%).

Obtaining and lyophilising CNF

CNF was obtained in a solution at a consistency of 1,5 % (w/w). The yield was calculated for freeze-drying the solution to obtain dry NCF. The yield was approximately 96 % from the milling of the cellulosic pulp. These results are consistent with the proper proportion of cellulose in the pulp.

The high, middle and basal sections achieved average cumulative yields (of the entire transformation from log to CNF) of 32,1 %, 33,6 % and 31 %, respectively. See Figure 1.

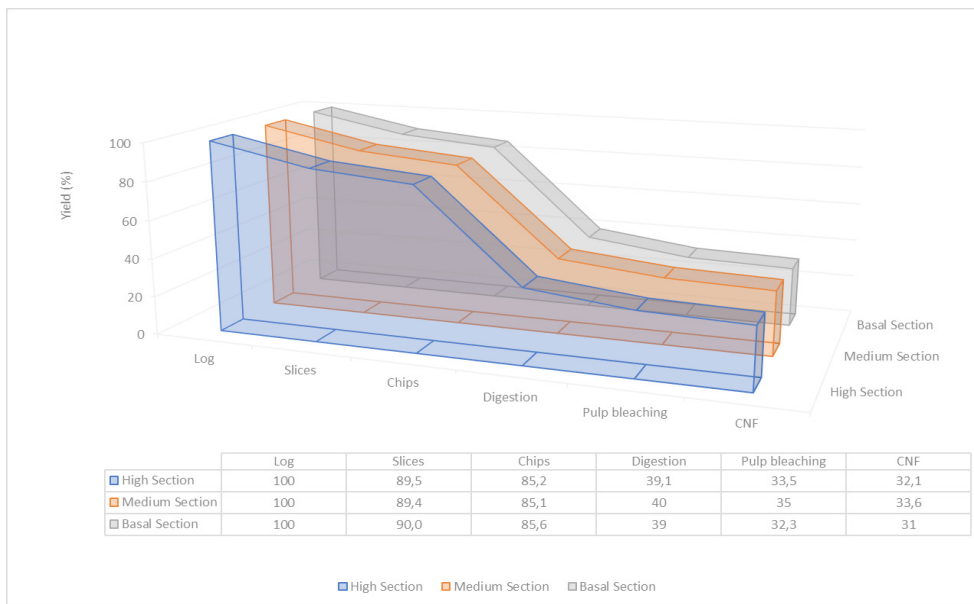


Figure 1: Cumulative performance in obtaining CNF from *Guazuma crinita* logs.

CNF characterisation

Determination of polymerisation degree (DP) of CNF

The DP of CNF presented significant differences in all the sections of origin. The values were 300, 249 and 211 for the basal, middle and high sections, respectively. A decrease in the DP of CNF was evidenced as the height of the section of origin increased.

This coincides with the discussion by Carballo *et al.* (2004), which mentions that, at greater stem height, fibres are less cross-linked with each other owing to a lower lignin content and less fibre development, thereby suggesting a lower DP of their composing monomeric units.

Tárres (2017) obtained DP values in the range between 300 and 450 for CNF from Eucalyptus via enzymatic hydrolysis (Endo- β -1,4-glucanase); Megashah *et al.* (2020) obtained DP values of 500 for oil palm CNF obtained using mechanical treatments such as disc milling, and Hu *et al.* (2015) obtained a DP of 660 for CNF from Eucalyptus. These results show that DP varies according to the material from which CNF is obtained and the treatment used for CNF production. In this context, the large-scale decrease in the obtained DP (between 210 and 300) was mainly due to the treatments to which the wood was subjected until obtaining CNF, with large influence mainly of the digestion, bleaching and final mechanical milling processes.

Scanning electron microscopy

The Figure 2a denotes the nanofibrils (indicated by red arrows) with a morphology very similar to the original fibres, but at a nanometer size in diameter, which may be due to the delignification level higher than 98 %, reason for which the nanofibrils had greater feasibility to be released by the shear forces produced by the impact of the moving balls on the paste.

Figure 2b depicts the nanofibrils released from the original fibres, which formed a network-like structure. Moreover, Figure 2c depicts rough surfaces (enclosed in red circles) that were present on the nanofibrils. Ramesh and Radhakrishnan (2019) have reported that surface roughness is due to the dissolution of lignin and hemicellulose compounds, removed during the alkaline hydrolysis and bleaching process. The appearance of roughness resulting from the loss of non-cellulosic components is due to sedimentation of the fibres in the plant cell wall by these components; consequently, when these components are removed, they leave the fibrils worn.

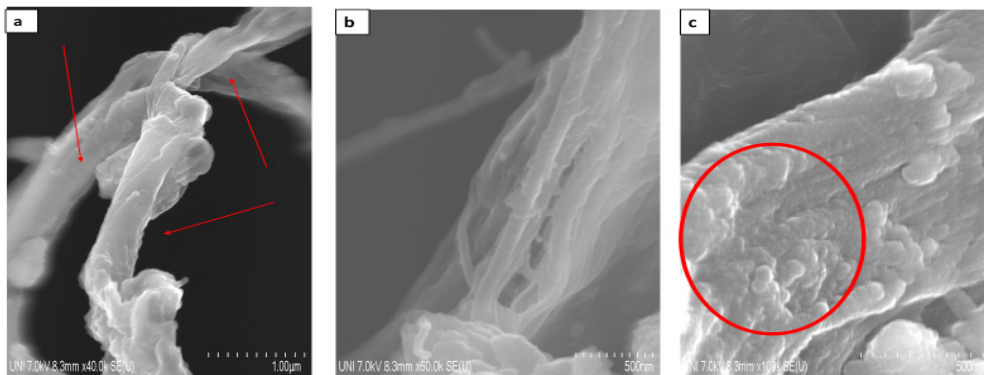


Figure 2: SEM micrographs of CNF of *Guazuma crinita* wood from different sections. (a) Cellulosic microfibril, (b) Macrofibril defibrillation and (c) Microfibril roughness.

Table 5 lists the average diameter values of the nanofibrils that were measured with origin in the different sections of interest.

Table 5: CNF diameter.

Section	N	Average diameter Mann – Whitney (nm)
High section	62	84 (a) (64,99)
Medium section	44	75 (b) (54,92)
Basal section	48	69 (b) (51,5)

N is the number of nanofibril bundles measured per section. () Coefficient of variation. Means that do not share a letter are significantly different.

Generally, nanofibrils with average diameters < 100 nm was obtained. Importantly, the diameter of the nanofibrils originating in the high section was larger than that of the nanofibrils originating in the middle and basal sections.

The results contrasted with those reported by Ponce *et al.* (2020), who obtained NCF from Tara with diameters of 300 nm using the same equipment for mechanical treatment, presenting higher values than those obtained in this study. This may be because they did not perform pulp bleaching; therefore, fibres were compacted even by the remaining lignin during defibrillation. Conversely, Siró and Plackett (2010) obtained NC from bleached pine pulp with diameters between 10 nm and 100 nm using a high-pressure homogeniser.

The difference in results with respect to those obtained by other authors is due to the different conditions during the mechanical disintegration of the cellulosic pulp, validating the study conducted by Fukuzumi *et al.* (2013), who assessed the dimensional change of the nanofibrils before evaluating different milling parameters.

Fourier transform infrared (FTIR) spectroscopy

Infrared (IR) spectra corresponding to each section were analysed using the averages of the absorbance obtained in the spectral range of 400 cm^{-1} - 4000 cm^{-1} . Figure 3 depicts the FTIR spectra of the CNF obtained from the high, middle and basal sections.

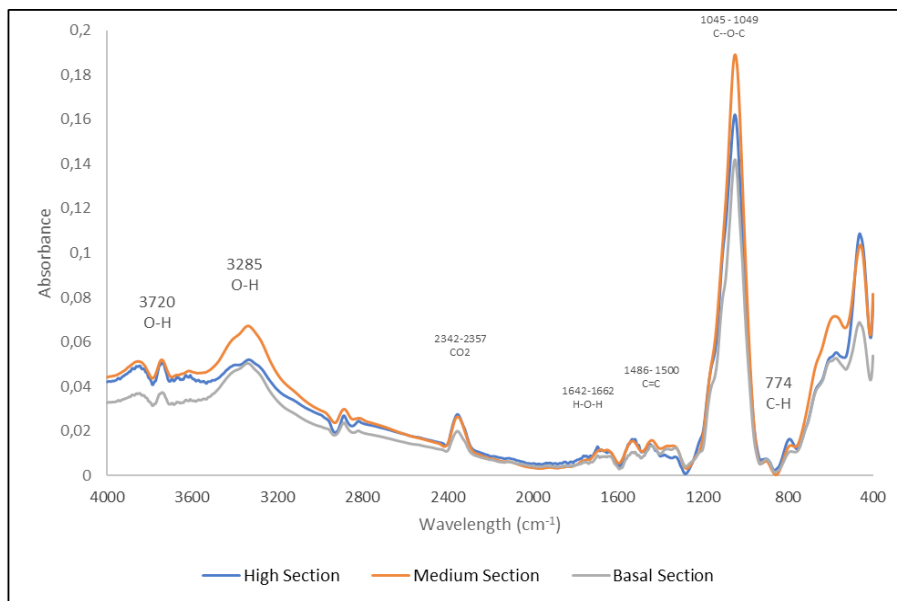


Figure 3: Infrared (IR) spectra of high, medium and basal section of CNF of *Guazuma crinita*.

The C-H bonds (770 cm^{-1} to 880 cm^{-1}) directly related to the vibrations of glycosidic bonds of glucose monomers were evidenced, which were also possible indicators of the remaining amorphous zone of cellulose (Hospodarova *et al.* 2018).

In this study, we were able to verify the presence of C–O–C bonds (1045 cm^{-1} – 1049

cm^{-1}) corresponding to the pyranose rings constituting cellulose, C=C bonds (1475 cm^{-1} – 1600 cm^{-1}) originating from the aromatic rings of lignin and CO_2 (weak absorptions very close to 2346 cm^{-1}), as CO_2 can be easily added on the surface of the study material through the adsorption phenomenon.

Furthermore, O–H bonds peaks (3000 cm^{-1} to 4000 cm^{-1}) originated from the hydroxyls present in the cellulose molecules in addition to the O–H bonds (1631 cm^{-1} – 1665 cm^{-1} and 3311 cm^{-1} – 3329 cm^{-1}) typical of the hydrogen bridge characteristic of intermolecular bonds between cellulose chains. For these bonds,

the absorptions were weak because the water in the CNF was removed via freeze-drying (Larkin 2018, Mandal and Chakrabarty 2011, Oancea *et al.* 2012, Rigg 2018). Additionally, the vibrational peak at 1049 cm^{-1} denotes a large stretch related to cellulose crystallinity (Elanthikkal *et al.* 2010, Hospodarova *et al.* 2018). Moreover, nearby peaks are present between 1630 cm^{-1} and 1730 cm^{-1} , which are representations of vibrations corresponding to acetyl and uronic ester bonds of hemicellulose and ester bonds present in carboxylic groups of lignin (Johar *et al.* 2012, Kumar *et al.* 2014).

As evidenced, the NaOH treatments during digestion and the NaClO and H_2O_2 used in bleaching had considerable effect on the oxidation and partial removal of non-cellulosic elements.

The IR spectra patterns showed no differences among the three zones, coinciding with the chemical characterisation (Table 1).

X-ray diffraction

From the obtained diffractograms (Figure 4), it was observed that the most distinct peaks were those present at $2\theta = 15,7^\circ$; $22,5^\circ$ and $34,7^\circ$, which correspond to (110), (200) and (004) crystalline planes respectively, typical of type I β cellulose. Moreover, this trend of peaks was much more evident for the basal and middle zones. For the high zone, no intensity peaks were found for $2\theta = 15,7^\circ$ but for $2\theta = 12,7^\circ$ and $14,4^\circ$, which were associated with the (110) plane of a crystalline region characteristic of type II cellulose. Based on the aforementioned X-ray diffraction observations, we inferred that the chemical treatment performed for the release of cellulose from other compounds exerted a more substantial effect on the high zone by disordering and/or somehow affecting the crystallinity of its structure.

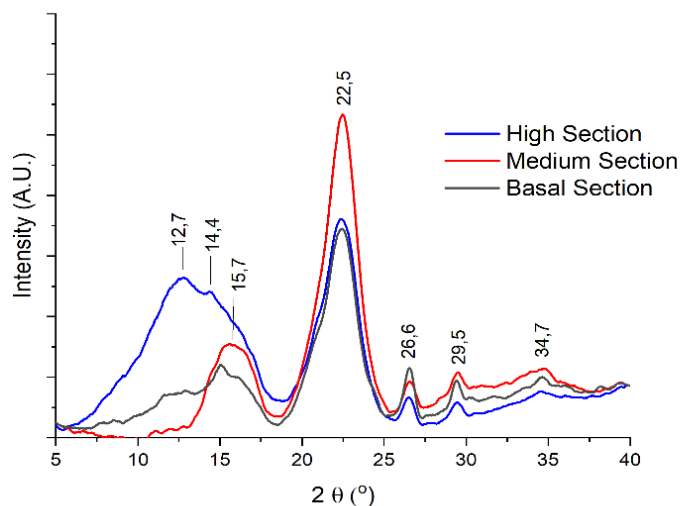


Figure 4: CNF diffractograms of *Guazuma crinita* obtained from three different sections of the longitudinal axis of the shaft.

The highest degree of crystallinity (IC) was obtained from the basal section with a value of 96 % (crystal diameter = 3,4 nm), followed by the middle zone with a value of 93 % (crystal diameter = 3,6 nm) and the high zone with a value of 76 % (crystal diameter = 3,4 nm). No correlation was found between the IC and the average crystal size of each CNF sample from each longitudinal section of the tree. Crystallinity values were high owing to the successive chemical treatments conducted to obtain CNF, which caused a decrease in the amorphous zones.

Overall, the obtained crystallinity index was above the crystallinity index range reported by Campano *et al.* (2016), who mention that for a fibrillar nanocellulosic material to have good mechanical and physical

properties, the crystallinity index must be between 84 % and 89 %. The decrease in CNF crystallinity with respect to the increase in shaft height exhibited the same trend with respect to DP. Hence, the number of monomers composing the cellulosic chain had a direct influence on the IC.

Thermogravimetric analysis

The decomposition of the NCF started from 250 °C and culminated at approximately 360 °C. In this range, the highest amount of mass (volatile material) was released with 82,1 % and 82,3 % for the CNF from the high and basal sections, respectively, for which these results did not show significant differences (Figure 5).

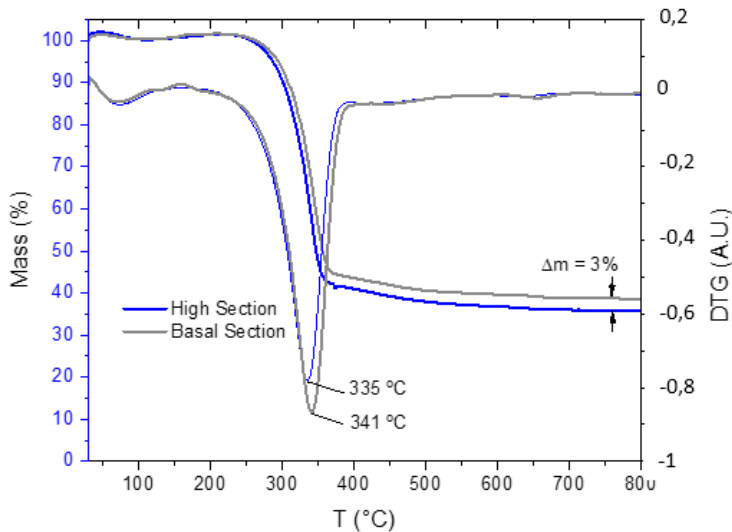


Figure 5: CNF thermograms obtained from the high and basal sections.

The temperature corresponding to the maximum decomposition rate for the CNF from the basal zone (341 °C) was higher with respect to that for the CNF from the high zone (335 °C), with a difference of 6 °C, where the sample from the apex lost a slightly higher mass percentage (approximately 3 %) than the sample from the base. This is due higher crystallinity values are related with lowest thermal degradation stability in CNF and CNC (Yildirim and Shaler 2017). This trend was related to the nanofibrils of the basal zone being more developed than those of the apex, which was corroborated by the polymerisation and crystallinity degree results because the sample of this zone was more rigid and therefore might have needed more energy for its decomposition compared with the high CNF.

Ultraviolet-visible spectroscopy

The results of methylene blue adsorption by CNF from different sections validate an efficiency > 60 % for the removal of methylene blue at different concentrations (10 ppm and 20 ppm) using CNF at two different weights of 50 mg and 100 mg (Table 6).

Table 6: Methylene blue removal values at different concentrations using CNF.

Initial concentration of methylene blue	Adsorbent mass	Section	Ce (mg/L)	qe (mg/g)
20 mg/L	50 mg	High	9,51	10,34
		Medium	10,06	9,97
		Basal	9,89	9,98
	100 mg	High	6,74	6,51
		Medium	7,07	6,47
		Basal	7,56	6,17
10 mg/L	50 mg	High	3,84	6,83
		Medium	4,14	6,52
		Basal	4,34	6,21
	100 mg	High	2,96	3,85
		Medium	3,04	3,78
		Basal	3,55	3,51

Ce: Equilibrium concentration and qe: Specific adsorption.

The adsorption capacity was considerably higher in the high zone with a value of 65 %, followed by the middle and basal zones, with values of 62 % and 61 %, respectively. This was due to the CNF from the high zone containing a higher proportion of amorphous zone in its structure, indicated by its much lower crystallinity index than the middle and basal zones; therefore, it has more availability to generate bonds with the molecules that compose the methylene blue reagent. Moreover, Keplinger *et al.* (2019) have reported that the adsorption capacity is influenced by the type of drying performed on NC, according to which supercritical drying as the lyophilisation used in this study yields better results by retaining the porous structure of NC without the use of any solvent.

By increasing the initial concentration of adsorbate (methylene blue) from 10 ppm to 20 ppm, the removal percentage decreased from 61,6 % to 50,8 % and from 70,2 % to 64,3 % for the adsorbent masses of 50 mg and 100 mg CNF, respectively. Because at a higher availability of available adsorption sites at low concentrations of the adsorbate, much of methylene blue molecules can be removed more effectively. However, when the initial concentration of the adsorbate is increased, the competition to attach to the available sites among the methylene blue molecules increases, and even after reaching equilibrium, these molecules remain in the solution, which reduces the removal percentage (Ahmad and Alrozi 2010, Rangabhashiyam *et al.* 2014).

CONCLUSIONS

CNF was obtained from bleached cellulosic pulp of bolaina blanca (*Guazuma crinita* Lam.) from different shaft sections. The wood to CNF yields were higher than 32 % for the different sections of the longitudinal axis of the shaft from which it was obtained.

CNF obtained from the different sections generally had a diameter < 90 nm. CNF from the high section had a considerably larger diameter than CNF from the middle and basal sections.

CNF from the basal section exhibited a considerably higher degree of polymerisation, more crystallinity and better thermostability. Moreover, CNF from the high section exhibited considerably better methylene blue dye adsorption condition.

Authorship contributions

S. A. A-P.: Data curation, formal analysis, investigation, methodology, software, validation, visualization, writing - original draft, writing - review & editing. H. E. G-M: Conceptualization, funding acquisition, supervision, project administration, resources, methodology, writing - original draft, writing - review & editing. S. P. P-A.: Writing - review & editing. A. A. G-E.: Writing - review & editing. A. J. C-O.: Conceptualization, funding acquisition, supervision, methodology, project administration, resources, writing - original draft, Writing - review & editing.

Acknowledgements

This work was elaborated thanks to the support of 009-2020-FONDECYT- BM project - Development of biodegradable and antibacterial packaging paper using a bilayer film based on nanocellulose from forest residues of bolaina blanca (*Guazuma crinita* Lam.) with the incorporation of copper nanoparticles for the food industry.

REFERENCES

- Ahmad, A.; Alrozi, R. 2010.** Optimization of preparation conditions for Mangosteen peel-based activated carbons for the removal of Remazol brilliant blue R using response surface methodology. *Chemical Engineering Journal* 165(3): 883-890. <https://doi.org/10.1016/j.cej.2010.10.049>
- ASTM. 2015.** Standard test methods for proximate analysis of coal and coke by macro thermogravimetric analysis. ASTM D7582-15. ASTM International: West Conshohocken, Pennsylvania, United States.
- Bajpai, P. 2018.** Chapter 12. Pulping Fundamentals. In: *Handbook of pulp and paper* (Third Ed.). Elsevier. <https://doi.org/10.1016/B978-0-12-814240-0.00012-4>
- Beeckman, H. 2016.** Wood anatomy and trait-based ecology. *IAWA Journal* 37(2): 127-151. <https://doi.org/10.1163/22941932-20160127>
- Borjesson, M.; Westman, G. 2015.** Chapter 7. Crystalline nanocellulose-preparation, modification and properties. In: *Cellulose - Fundamental Aspects and Current Trends*. IntechOpen. <http://dx.doi.org/10.5772/61899>
- Campano, C.; Balea, A.; Blanco, A.; Negro, C. 2016.** Enhancement of the fermentation process and properties of bacterial cellulose: a review. *Cellulose* 23(1): 57-91. <https://doi.org/10.1007/s10570-015-0802-0>
- Carballo, L.; Orea, U.; Cordero, E. 2004.** Composición química de tres maderas en la provincia de Pinar Del Río, CUBA a tres alturas del fuste comercial, Parte 4: Estudio comparativo de la composición química. *Revista Chapingo Serie Ciencias Forestales y del Ambiente* 10(2): 77-81. <https://revistas.chapingo.mx/forestales/?section=articles&subsec=issues&numero=30&articulo=414>
- Césare, M.; Hilario, F.; Callupe, N.; Cruz, L.; Calle, J.; Gonzales, H. 2019.** Caracterización química y física del bambú. *Avances en Ciencias e Ingeniería* 10(4): 1-13. <https://www.executivebs.org/publishing.cl/aci/2019/Vol10/Nro4/1-ACI1336-19-full.pdf>
- Cipra Rodriguez, J.A.; Gonzales Mora, H.E.; Cárdenas Oscanoa, A.J. 2022.** Characterization of MDF produced with bolaina (*Guazuma crinita* Mart.) wood residues from plantation. *Madera Bosques* 28(3): e2832433. <https://doi.org/10.21829/myb.2022.2832433>
- Córdova, A.; Cárdenas, A.; Gonzáles, H. 2020.** Caracterización física y mecánica de compuestos de *Guazuma crinita* Mart. a base de polipropileno virgen. *Revista Mexicana de Ciencias Forestales* 11(57): 1-28. <https://doi.org/10.29298/rmcf.v11i57.621>

Elanthikkal, S.; Gopalakrishnanpanicker, U.; Varghese, S.; Guthrie, J.T. 2010. Cellulose microfibrils produced from banana plant wastes: Isolation and characterization. *Carbohydrate Polymers* 80(3): 852-859. <https://doi.org/10.1016/j.carbpol.2009.12.043>

Fukuzumi, H.; Saito, T.; Isogai, A. 2013. Influence of TEMPO- oxidized cellulose nanofibril length on film properties. *Carbohydrate Polymers* 93: 172-177. <https://doi.org/10.1016/j.carbpol.2012.04.069>

Habibi, Y. 2014. Key advances in the chemical modification of nanocelluloses. *Chemical Society Reviews* 43(5): 1519-1542. <https://doi.org/10.1039/C3CS60204D>

Herrera, M. 2018. Obtención de nanocelulosa a partir de celulosa de puntas de abacá. Engineering thesis. Escuela Politécnica Nacional. Quito, Ecuador. <https://bibdigital.epn.edu.ec/handle/15000/19544>

Honorato, A.; Colotl, G.; Apolinar, F.; Aburto, J. 2015. Principales componentes químicos de la madera de Ceiba pentandra, *Hevea brasiliensis* y *Ochroma pyramidale*. *Maderas Bosques* 21(2): 131-146. <https://doi.org/10.21829/myb.2015.212450>

Hospodarova, V.; Singovszka, E.; Stevulova, N. 2018. Characterization of Cellulosic Fibers by FTIR Spectroscopy for Their Further Implementation to Building Materials. *American Journal of Analytical Chemistry* 9(6): 303-310. <https://doi.org/10.4236/ajac.2018.96023>

Hu, C.; Zhao, Y.; Li, K.; Zhu, J.Y.; Gleisner, R. 2015. Optimizing cellulose fibrillation for the production of cellulose nanofibrils by a disk grinder. *Holzforschung* 69(8): 993-1000. <https://doi.org/10.1515/hf-2014-0219>

IAWA. 1989. IAWA list of microscopic features for hardwood identification with an appendix on non-anatomical information. Wheeler, E.A.; Baas, P.; Gasson, P.E. (Eds.). Published for the International Association of Wood Anatomists at the National Herbarium: Netherlands, Leiden. *IAWA Journal* 10(3): 219-332. <https://www.iawa-website.org/uploads/soft/Abstracts/IAWA%20list%20of%20microscopic%20features%20for%20hardwood%20identification.pdf>

IBAMA. 1991. Normas de procedimentos em estudos do anatomia do madeira: I. Angiospermae. 19p. <https://lpf.florestal.gov.br/pt-br/publicacoes-tecnicas-do-lpf/72-normas-de-procedimentos-em-estudos-de-anatomia-de-madeira-i-angiospermae-ii-gimnospermae>

Johar, N.; Ahmad, I.; Dufresne, A. 2012. Extraction, preparation and characterization of cellulose fibres and nanocrystals from rice husk. *Industrial Crops and Products* 37(1): 93-99. <https://doi.org/10.1016/j.indcrop.2011.12.016>

Kargarzadeh, H.; Ioelovich, M.; Ahmad, I.; Thomas, S.; Dufresne, A. 2017. Methods for extraction of nanocellulose from Various Sources. Chapter 1. In *Handbook of nanocellulose and cellulose Nanocomposites*. Wiley-VCH. <https://doi.org/10.1002/9783527689972.ch1>

Katahira, R.; Elder, T.J.; Beckham, G.T. 2018. Brief introduction to lignin structure. Chapter 1. In *Lignin Valorization: Emerging Approaches*. Beckham, G.T. (Ed.). Energy and Environment Series No. 19. 1-20. The Royal Society of Chemistry. <https://books.rsc.org/books/edited-volume/625/chapter/307517/A-Brief-Introduction-to-Lignin-Structure>

Keplinger, T.; Wang, X.; Burgert, I. 2019. Nanofibrillated cellulose composites and wood derived scaffolds for functional materials. *Journal of Materials Chemistry A* 7: 2981-2992. <https://doi.org/10.1039/c8ta10711d>

Kumar, A.; Negi, Y.S.; Choudhary, V.; Bhardwaj, N.K. 2014. Characterization of cellulose nanocrystals produced by acid-hydrolysis from sugarcane bagasse as agro-waste. *Journal of Materials Physics and Chemistry* 2(1): 1-8. <https://doi.org/10.12691/jmpc-2-1-1>

Larkin, P.J. 2018. IR and Raman Spectra-Structure Correlations: Characteristic Group Frequencies. Chapter 6. In *Infrared and Raman spectroscopy: principles and spectral interpretation*. Second Ed. 85-134p. Elsevier International Publishing. <https://doi.org/10.1016/B978-0-12-804162-8.00006-9>

Lee, K.Y.; Tang, M.; Williams, C.K.; Bismarck, A. 2012. Carbohydrate derived copoly(lactide) as the compatibilizer for bacterial cellulose reinforced polylactide nanocomposites. *Composites Science and Technology* 72(14): 1646-1650. <https://doi.org/10.1016/j.compscitech.2012.07.003>

Lermen, A.M.; Fronza, C.S.; Diel, J.C.; Schein, D.; Clerici, N.J.; Guimarães, R.E.; Boligon, S.D.; Scher, A.C. 2021. A utilização de resíduos agroindustriais para adsorção do corante azul de metileno: uma breve revisão. *Brazilian Applied Science Review* 5(1): 273-288. <https://doi.org/10.34115/basrv5n1-017>

Malpartida, I. 2010. Determinación de la composición química de la especie bolaina blanca (*Guazuma crinita* Mart.) procedente del sector cadena- Tingo María. Engineering thesis, Universidad Nacional Agraria de la Selva. Tingo María, Perú. <https://hdl.handle.net/20.500.14292/556>

Mandal, A.; Chakrabarty, D. 2011. Isolation of nanocellulose from waste sugarcane bagasse (SCB) and its characterization. *Carbohydrate Polymers* 86(3): 1291-1299. <https://doi.org/10.1016/j.carbpol.2011.06.030>

Manzano, D. 2021. Extracción de celulosa a partir de la especie *Calamagrostis intermedia* para la preparación de compuestos semisintéticos. Master Thesis, Universidad Técnica de Ambato. Ambato, Ecuador. <https://repositorio.uta.edu.ec/jspui/handle/123456789/32958>

Megashah, L.; Ariffin, H.; Zakaria, M.; Hassan, M.; Andou, A.; Padzil, F. 2020. Modification of cellulose degree of polymerization by superheated steam treatment for versatile properties of cellulose nanofibril film. *Cellulose* 27(13): 7417-7429. <https://doi.org/10.1007/s10570-020-03296-2>

Miguel, M.; Iwakiri, S.; Trianoski, R.; Gonzales, H.; Miguel, C. 2019. Producción de tableros de partículas con bolaina (*Guazuma crinita* Mart.) procedente de una plantación de cuatro años. *Brazilian Journal of Wood Science* 10(2): 197-204. <https://doi.org/10.12953/2177-6830/rcm.v10n3p197-204>

Oancea, A.; Grasset, O.; Le Menn, E.; Bollengier, O.; Bezacier, L.; Le Mouelic, S.; Tobie, G. 2012. Laboratory infrared reflection spectrum of carbon dioxide clathrate hydrates for astrophysical remote sensing applications. *Icarus* 221(2): 900-910. <https://doi.org/10.1016/j.icarus.2012.09.020>

Ozen, E.; Yildirim, N.; Dalkilic, B.; Ergun, M. 2021. Effects of microcrystalline cellulose on some performance properties of chitosan aerogels. *Maderas. Ciencia y Tecnología* (23): 1-10. <https://dx.doi.org/10.4067/s0718-221x2021000100426>

Ponce, S.; Chavarria, M.; Norabuena, F.; Chumpitaz, D.; Gutarra, A. 2020. Cellulose microfibrils obtained from agro-industrial Tara waste for dye adsorption in water. *Water, Air, & Soil Pollution* 231: e518. <https://doi.org/10.1007/s11270-020-04889-0>

Rangabhashiyam, S.; Anu, N.; Giri, M.; Selvaraju, N. 2014. Relevance of isotherm models in biosorption of pollutants by agricultural byproducts. *Journal of Environmental Chemical Engineering* 2(1): 398-414. <https://doi.org/10.1016/j.jece.2014.01.014>

Rodríguez, R.; Ramírez, A.; Palacios, H.; Fuentes, F.; Silva, J.; Saucedo, A. 2015. Características anatómicas, físico-mecánicas y de maquinado de la madera de mezquite (*Prosopis velutina* Wooton). *Revista Mexicana de Ciencias Forestales* 6(28): 156-173. https://www.scielo.org.mx/scielo.php?script=sci_arttext&pid=S2007-11322015000200011

Ramesh, S.; Radhakrishnan, P. 2019. Cellulose nanoparticles from agro-industrial waste for the development of active packaging. *Applied Surface Science* 484: 1274-1281. <https://doi.org/10.1016/j.apusc.2019.04.003>

Revilla, J. 2015. Viabilidad económica de plantaciones demostrativas de Bolaina blanca (*Guazuma crinita* C. Mart.) en la cuenca del río Aguaytía, Ucayali -Perú. Master Thesis, Escuela de Posgrado, Universidad Nacional Agraria la Molina. Lima, Perú <http://repositorio.lamolina.edu.pe/handle/20.500.12996/2119>

Rigg, P. 2018. Efecto de la adición de micro-nanocelulosa cristalina en adhesivos y su aplicación en aglomerados de madera de especies forestales tropicales. Master Thesis, Escuela de Ingeniería Forestal, Instituto Tecnológico de Costa Rica. Cartago, Costa Rica. https://repositoriotec.tec.ac.cr/bitstream/handle/2238/9783/efecto_adición_micronanocelulosa_cristalina_adhesivos.pdf?sequence=1&isAllowed=y

Siddiqui, N.; Mills, R.; Gardner, D.; Bousfield, D. 2011. Production and Characterization of Cellulose Nanofibers from Wood Pulp. *Journal of Adhesion Science and Technology* 25(6-7): 709-721. <https://doi.org/10.1163/016942410X525975>

Segal, L.; Creely, J.; Martin, A.; Conrad, C. 1959. An empirical method for estimating the degree of crystallinity of native cellulose using the X-ray diffractometer. *Textile Research Journal* 29(10): 786-764. <https://doi.org/10.1177/004051755902901003>

Singh, K.; Matsagar, B.; Dhepe, P. 2021. Determination of alpha-, beta-and gamma-cellulose in bagasse and wheat Straw: lignin recovery, characterization and depolymerization. *Clean Technologies and Environmental Policy* 19: 23-29. <https://doi.org/10.21203/rs.3.rs-193157/v1>

Siró, I.; Plackett, D. 2010. Microfibrillated cellulose and new nanocomposite materials: a review. *Cellulose* 17(3): 459-494. <https://doi.org/10.1007/s10570-010-9405-y>

TAPPI. 2008. Viscosity of pulp (capillary viscometer method). TAPPI T230 om-08. The Technological Association of the pulp and paper Industry: Atlanta, GA, USA.

TAPPI. 2007. Solvent extractives of wood and Pulp. TAPPI T 204 om. The Technological Association of the pulp and paper Industry. Atlanta, GA. USA.

TAPPI. 1998. Acid-insoluble lignin in wood and Pulp. TAPPI T 222 om. The Technological Association of the pulp and paper Industry. Atlanta, GA. USA.

TAPPI. 1993a. Ash in wood, pulp, paper and paperboard: combustion at 525°C. TAPPI T 211 om. The Technological Association of the pulp and paper Industry: Atlanta, GA. USA.

TAPPI. 1993b. Kappa number of pulp. TAPPI T 236 om. The Technological Association of the pulp and paper Industry: Atlanta, GA, USA.

Tárres, J.A. 2017. Endo- β -1,4-glucanasa para la fabricación de micro/nanocelulosa: propiedades y aplicaciones. Doctoral thesis, Universitat de Girona. Girona, España. <http://www.tdx.cat/handle/10803/456211>

Trache, D.; Tarchoun, A.; Derradji, M.; Hamidon, T.; Masruchin, N.; Brosse, N.; Hussin, M. 2020. Nanocellulose: from fundamentals to advanced applications. *Frontiers in Chemistry* 8: e392. <https://doi.org/10.3389/fchem.2020.00392>

Yildirim, N.; Shaler, S. 2017. A Study on Thermal and Nanomechanical Performance of Cellulose Nanomaterials (CNs). *Materials* 10: e718. <https://doi.org/10.3390/ma10070718>

Zaki, J.; Muhammed, S.; Shafie, A.; Wan, W. 2012. Chemical properties of juvenile latex timber clone rubberwood trees. *The Malaysian Journal of Analytical Sciences* 16(3): 228-234. <http://mjas.analis.com.my/wp-content/uploads/2018/11/Junaiza.pdf>